
[View Journal Online](#)
[View Article Online](#)

Rationale design and synthesis of some novel imidazole linked thiazolidinone hybrid molecules as DNA minor groove binders

 Javeed Ahmad War * and Santosh Kumar Srivastava 

Synthetic Organic Chemistry and Molecular Modelling Laboratory, Department of Chemistry, Dr. Hari Singh Gour University, Sagar, Madhya Pradesh, 470003, India

javeedahmadwar@yahoo.com (J.A.W.), profksgr@gmail.com (S.K.S.)

* Corresponding author at: Synthetic Organic Chemistry and Molecular Modelling Laboratory, Department of Chemistry, Dr. Hari Singh Gour University, Sagar, Madhya Pradesh, 470003, India

 e-mail: javeedahmadwar@yahoo.com (J.A. War).

RESEARCH ARTICLE

ABSTRACT



doi 10.5155/eurjchem.11.2.120-132.1974

Received: 24 February 2020

Received in revised form: 01 April 2020

Accepted: 03 April 2020

Published online: 30 June 2020

Printed: 30 June 2020

KEYWORDS

 Thiourea
 Imidazole
 BSA binding
 DNA binding
 Molecular docking
 Antimicrobial activity

A new series of imidazole linked thiazolidinone hybrid molecules was designed and subsequently synthesized through a feasible, three step reaction protocol. The structures of these molecules were established using FT-IR, ¹H NMR, ¹³C NMR and HRMS techniques. *In vitro* susceptibility tests against some Gram positive (*Staphylococcus aureus* and *Bacillus subtilis*) and Gram negative bacteria (*Escherichia coli* and *Pseudomonas aeruginosa*) exhibited broad spectrum potency of the molecules. The most potent molecule (S2A7) amongst the screened molecules, showed minimum inhibitory concentration (MIC) value not less than 2.0 µg/mL which was at par with the reference drug Streptomycin. Structure activity relationships revealed nitro and chloro groups being crucial for bioactivity when present at meta position of arylidene ring in 3-(3-(imidazol-1-yl)propyl)-5-(benzylidene)-2-(phenylimino)thiazolidin-4-one. Deoxyribonucleic acid (DNA) and bovine serum albumin (BSA) binding studies for S2A7 under simulated physiological pH were probed using UV-Visible, fluorescence quenching, gel electrophoresis and molecular docking techniques. These studies established that S2A7 has strong binding affinity towards DNA and binds at the minor groove of DNA with binding constant (K_b) of 0.1287×10^2 L/mol. Molecular docking simulations of S2A7 with DNA and BSA predicted binding affinity of -9.2 and -7.2 kcal/mol, respectively. Van der Waals forces and hydrogen bonding interactions were predicted as the main forces of interaction. With DNA, S2A7 exhibited specific binding affinity towards adenine-thiamine base pairs. The compound S2A7 forms a stable complex with BSA by binding at subdomain IIIA implying high bio-distribution of the compound.

 Cite this: *Eur. J. Chem.* 2020, 11(2), 120-132

 Journal website: www.eurjchem.com

1. Introduction

With advancements in the field of medicinal chemistry, new classes of antimicrobial drugs were discovered and later clinically used. Initially these drugs met with huge clinical success in treating patients with bacterial infections and related diseases [1]. However, over time, microbes developed resistance making these drugs less effective [2]. Microbes develop resistance either by erroneous replication or by exchange of resistant traits among themselves [3]. The 2014 global report of World Health Organization (WHO) on antimicrobial resistance (AMR) warns AMR as a global threat. The report specifically mentions that resistance of common bacteria to commercial antibiotics has reached alarming levels in many parts of the world. The report highlights that resistance to most widely used antibacterial medicines, fluoroquinolones and methicillin for the treatment of infections caused by *E. coli* and *S. aureus*, respectively, is very widespread [4]. This scenario poses a huge challenge and at the same times, an opportunity of developing new classes of antibiotics which could be effective against the resistant microbial strains, either because of higher inhibitory nature or due to different mechanism of action than are for the existing drugs.

Imidazole is a versatile ring with paramount biological importance [5-7] which is evident from the fact that it constitutes skeleton of many commercial drugs (Figure 1) viz. metronidazole (antimicrobial), antifungal imidazole drugs, cimetidine (Histamine H₂-receptor antagonist) and flumazenil (GABA_A receptor antagonist). Imidazole polyamides constitute a highly active structural group which show anti-cancer activity by binding at DNA minor groove [8,9]. Likewise, the chemistry of thiazolidine ring system is of considerable interest as it forms core structure of many biomolecules, commercial drugs and synthetic molecules with promising antimicrobial, antifungal, anticancer and antidiabetic activity [10-13]. For decades the art of combing multiple pharmacophoric units into a single molecule has been established as a successful model to design new drug candidates, in structure-based drug design approach [14]. However, in spite of their huge pharmacophoric potential, there have been very few attempts to design hybrid molecules containing both imidazole and thiazolidinone moieties [7,15-16]. Keeping this in view and continuing our effort of building novel biologically active molecules [17,18], here we report some novel imidazole linked thiazolidinone hybrid molecules with the hypothesis

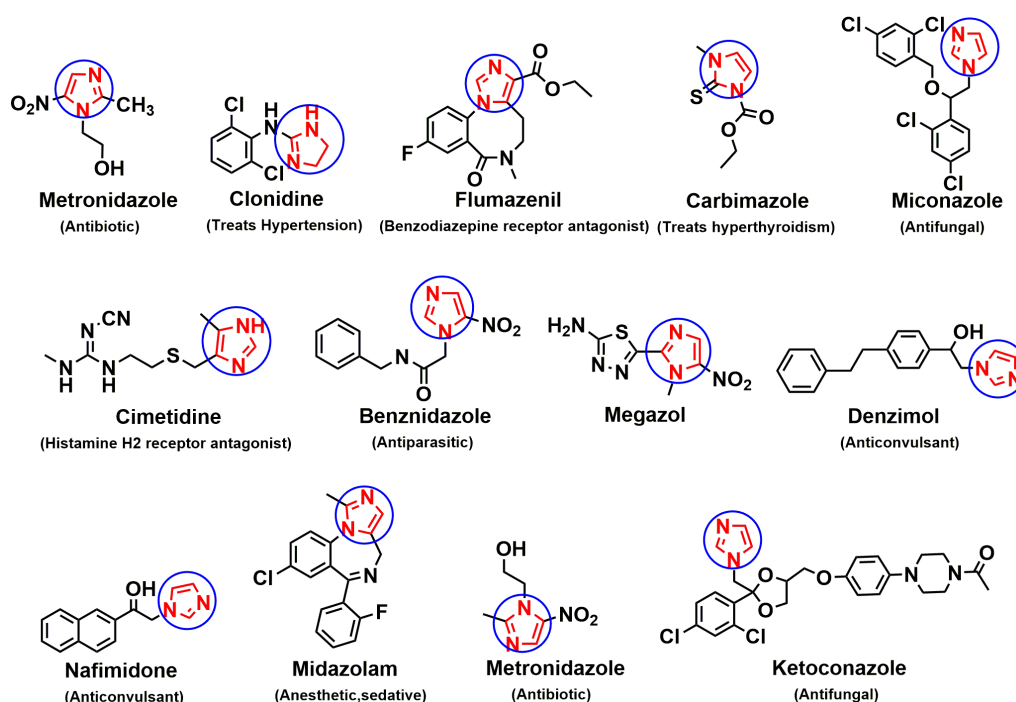


Figure 1. Structures of some clinically used drugs containing imidazole moiety.

that the resulting molecules would bear broad spectrum antibiotic applicability.

The designed molecules were synthesized through a three-step reaction protocol which involves simple reaction setup and moderate reaction conditions. *In vitro* antimicrobial activity was carried against some Gram positive (*Staphylococcus aureus* and *Bacillus subtilis*) and Gram-negative bacteria (*Escherichia coli* and *Pseudomonas aeruginosa*) through disc diffusion and agar dilution susceptibility tests. The commercial antibiotics which are presently in use have different mechanisms of action. While acting on the bacteria they either kill the bacteria (bactericidal) or stop its growth (bacterostatic). They do so by binding at cellular targets and inhibiting their normal function. The common cellular targets being peptidoglycons in cell wall synthesis, plasma membrane, ribosomes in protein synthesis, translation, transcription, DNA/RNA replication pathway and metabolites of cell [19]. DNA is a well known target for many commercial antibiotics. Metronidazole and nitrofurantoin for instance are commercial imidazole-based antibiotics which target DNA and modify its structure. Many other imidazole and thiazolidinone based molecules reported in literature have shown strong affinity towards DNA thereby inhibiting its function [20-22]. Encouraged by these reports, we decided to probe DNA as possible target for the synthesized molecules. Drugs may interact with DNA either by covalent or non-covalent binding. In non-covalent binding, which is the case with most of the synthetic organic molecules [23], the molecules usually interact with DNA in three ways viz; groove binding, intercalation or electrostatic interaction [24]. UV-Visible absorption, fluorescence quenching, gel electrophoresis and molecular modeling techniques were employed to study interaction with DNA. Bovine serum albumin (BSA) being the major soluble protein constituent of circulatory system, has many physiological functions and plays a key role in the transport of many endogenous and exogenous ligands. A drug molecule must have strong affinity towards BSA so as to increase its bioavailability. Spectral and *in silico* studies were carried to probe interaction of S2A7 with BSA.

2. Experimental

2.1. Materials and instrumentations

Starting materials, reagents and solvents were purchased either from Merck or from Aldrich (SK Traders, Indore, MP, India) and were of reagent grade. Chemicals required for biological tests were purchased from HiMedia, India. Compounds were synthesized mostly under reflux conditions. Melting points were determined on an open capillary apparatus and are reported without correction. Infrared spectra were recorded on Shimadzu FT-IR DR800 spectrophotometer with resolution of 2 cm^{-1} in the range of $400\text{-}4000\text{ cm}^{-1}$. ^1H NMR spectra of compounds in $\text{DMSO-}d_6$ were recorded on a Bruker AV 500 spectrometer (Bruker, Karlsruhe, Germany) at 500 MHz. Peak multiplicities are designed as: s, singlet; d, doublet; t, triplet; m, multiplet; dd, double doublet. Chemical shifts are reported as δ (ppm) relative to TMS as internal standard. High-resolution mass spectrometry was performed under ESI conditions at a resolution of 61800 using a Thermo Scientific exactive mass spectrometer. Elemental analysis was done by Thermo Scientific FLASH-2000 CHN Analyzer. The values were within 0.4% of the calculated values. The reactions were monitored by TLC on F_{254} silica-gel pre coated sheets (Merck, Darmstadt, Germany) which were visualized under UV (254 and 365 nm) light, with ethyl acetate:hexane (6:4, v:v) or chloroform:methanol (9:1, v:v) as solvent systems. The compounds were purified either by recrystallization or by column chromatography with 200-250 mesh silica gel.

2.2. Synthesis

2.2.1. General procedure for the synthesis of 1-(3-(1H-imidazol-1-yl)propyl)-3-phenylthiourea (S2A1)

Phenylisothiocyanate (15 g, 111.11 mmol) was dissolved in chloroform and equimolar amount of amine (13.89 g, 111.11 mmol) was added slowly at room temperature, and

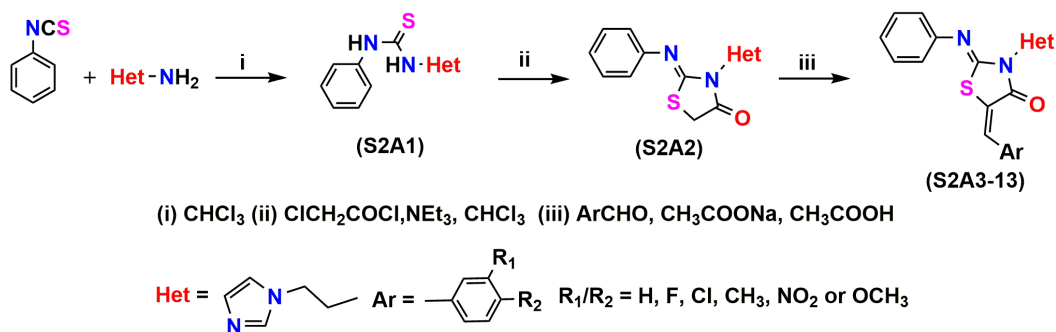


Figure 2. Reaction scheme for the synthesis of compound S2A1-13.

refluxed for 8 hours to get the product. The product was collected by filtration, washed with chloroform, dried and recrystallized from ethanol (95%) to afford product (S2A1) as white powder. The crude product was purified by column chromatography using chloroform:methanol (4:1, v:v) as eluent to afford the purified compound S2A1 (Figure 2).

1-(3-(1H-imidazol-1-yl)propyl)-3-phenylthiourea (S2A1): Color: White. Yield: 90%. M.p.: 275-278 °C. FT-IR (KBr, ν , cm^{-1}): 3390, 3273 (NH, thiourea), 3063 (CH_{Ar}). ^1H NMR (500 MHz, $\text{DMSO}-d_6$, δ , ppm): 9.50 (s, 1H, ^{11}NH), 7.79 (s, 1H, ^9NH), 7.62 (s, 1H, ^1CH), 7.40 (dd, 2H, $^{13,17}\text{CH}$, $J = 7.44, 1.04$ Hz), 7.30 (td, 2H, $^{14,16}\text{CH}$, $J = 8.28, 7.44$), 7.14 (d, 1H, ^4CH , $J = 7.54$ Hz), 7.09 (td, 1H, ^{15}CH , $J = 7.36, 7.32$ Hz), 6.89 (d, 1H, ^3CH , $J = 7.36$ Hz), 4.01 (t, 2H, $^6\text{CH}_2$, $J = 6.96, 7.0$ Hz), 3.49 (t, 2H, $J = 4.96, 6.0$ Hz, $^8\text{CH}_2$), 2.02 (m, 2H, $^7\text{CH}_2$). ^{13}C NMR (125 MHz, $\text{DMSO}-d_6$, δ , ppm): 180.57 (^{10}C), 139.06 (^{12}C), 137.09 (^1C), 128.51 ($^{14,16}\text{C}$), 128.35 (^{15}C), 124.14 (^3C), 123.21 ($^{13,17}\text{C}$), 119.12 (^4C), 43.84 (^6C), 41.15 (^8C), 30.11 (^7C). HRMS (ESI, m/z) calcd. for $\text{C}_{13}\text{H}_{16}\text{N}_4\text{S}$, 260.11; found 260.12056.

2.2.2. General procedure for the synthesis of 3-(3-(1H-imidazol-1-yl)propyl)-2-(phenylimino)thiazolidin-4-one (S2A2)

To a solution of compound S2A1 (15g, 97.08 mmol) in chloroform (80mL), a slightly excess of chloroacetyl chloride was added drop wise in presence of catalytic amount of NEt_3 . The mixture was refluxed till the completion of the reaction (18 hours) as monitored by TLC. The solvent was evaporated. Removal of the solvent gives an oily residue, which was dissolved in diethyl ether and repeatedly washed with aqueous sodium carbonate (10%). The organic layer was dried over sodium sulfate, filtered, and concentrated to afford the compound S2A2 (Figure 2).

3-(3-(1H-imidazol-1-yl)propyl)-2-(phenylimino)thiazolidin-4-one (S2A2): Color: White. Yield: 85%. M.p.: 352-357 °C. FT-IR (KBr, ν , cm^{-1}): 3061 (CH_{Ar}), 1730 (C=O), 1570 (C=N), 1269 (NCS ring). ^1H NMR (500 MHz, $\text{DMSO}-d_6$, δ , ppm): 7.65 (s, 1H, ^1CH), 7.09 (d, 1H, ^4CH , $J = 7.35$ Hz), 7.15-7.45 (m, 5H, Ar-H), 6.85 (d, 1H, ^3CH , $J = 7.20$ Hz), 4.21 (s, 2H, $^{11}\text{CH}_2$), 4.10 (t, 2H, $^6\text{CH}_2$, $J = 6.96, 7.0$ Hz), 3.40 (t, 2H, $^8\text{CH}_2$, $J = 6.21, 5.20$ Hz), 2.15 (m, 2H, $^7\text{CH}_2$). ^{13}C NMR (125 MHz, $\text{DMSO}-d_6$, δ , ppm): 182.50 (^{10}C), 157.28 (^{13}C), 140.26 (^{15}C), 135.19 (^1C), 129.55 ($^{16,20}\text{C}$), 126.55 (^{18}C), 126.27 (^3C), 125.26 ($^{17,19}\text{C}$), 122.37 (^4C), 57.37 (^{11}C), 45.85 (^6C), 42.50 (^8C), 30.24 (^7C). HRMS (ESI, m/z) calcd. for $\text{C}_{15}\text{H}_{16}\text{N}_4\text{OS}$, 300.10; found 300.10156.

2.2.3. General procedure for the synthesis of 3-(3-(1H-imidazol-1-yl)propyl)-5-(substituted benzylidene)-2-(phenylimino)thiazolidin-4-one (S2A3-13)

To a solution of S2A2 (5 g, 16.65 mmol) in acetic acid/sodium acetate buffer (50 mL), different aromatic aldehydes

(1.5 equivalents) were added in separate reaction flasks and refluxed for 6-8 hours. The progress of reactions was monitored by TLC. After completion of the reactions, reaction mixtures were allowed to cool at room temperature; products were filtered and recrystallized from ethanol. Further purification was done by column chromatography with ethyl acetate:hexane (6:4, v:v) as eluent. Similar procedures were followed for the synthesis of morpholine based series (S2B1-13) (Figure 2).

3-(3-(1H-imidazol-1-yl)propyl)-5-benzylidene-2-(phenylimino)thiazolidin-4-one (S2A3): Color: Light brown. Yield: 70%. M.p.: 384-387 °C. FT-IR (KBr, ν , cm^{-1}): 3058 (CH_{Ar}), 1710 (C=O), 1680 (C=N), 1288 (NCS ring). ^1H NMR (500 MHz, $\text{DMSO}-d_6$, δ , ppm): 7.65 (s, 1H, ^1CH), 7.25 (d, 1H, ^4CH , $J = 7.10$ Hz), 7.20 (s, 1H, ^{21}CH), 7.10-6.95 (m, 10H, Ar-H), 6.90 (d, 1H, ^3CH , $J = 7.25$ Hz), 4.25 (t, 2H, $^6\text{CH}_2$, $J = 6.50, 7.1$ Hz), 3.58 (t, 2H, $^8\text{CH}_2$, $J = 5.12, 6.20$ Hz), 2.26 (m, 2H, $^7\text{CH}_2$). ^{13}C NMR (125 MHz, $\text{DMSO}-d_6$, δ , ppm): 181.50 (^{10}C), 157.28 (^{13}C), 141.15 (^{15}C), 135.29 (^1C), 129.25 (^{18}C), 129.15 ($^{16,20}\text{C}$), 126.26 (^3C), 124.10 ($^{17,19}\text{C}$), 121.35 (^4C), 57.35 (^{21}C), 57.14 ($^{23,27}\text{C}$), 57.12 (^{25}C), 57.10 ($^{24,26}\text{C}$), 57.10 (^{22}C), 56.53 (^{11}C), 45.17 (^6C), 40.23 (^8C), 32.10 (^7C). HRMS (ESI, m/z) calcd. for $\text{C}_{22}\text{H}_{20}\text{N}_4\text{OS}$ 388.14; found 388.13856.

(2Z, 5Z)-3-(3-(1H-imidazol-1-yl)propyl)-5-(3-fluorobenzylidene)-2-(phenylimino)thiazolidin-4-one (S2A4): Color: Light brown. Yield: 65%. M.p.: 400-403 °C. FT-IR (KBr, ν , cm^{-1}): 1710 (C=O), 1628 (C=N), 1210 (C-F). ^1H NMR (500 MHz, $\text{DMSO}-d_6$, δ , ppm): 7.65 (s, 1H, ^1CH), 7.25 (d, 1H, ^4CH , $J = 7.10$ Hz), 7.14-6.95 (m, 9H, Ar-H), 7.15 (s, 1H, ^{21}CH), 6.90 (d, 1H, ^3CH , $J = 7.25$ Hz), 4.25 (t, 2H, $^6\text{CH}_2$, $J = 6.50, 7.1$ Hz), 3.80 (s, 2H, $^8\text{CH}_2$), 2.26 (m, 2H, $^7\text{CH}_2$). ^{13}C NMR (125 MHz, $\text{DMSO}-d_6$, δ , ppm): 171.05 (^{10}C), 164.51 (^{24}C), 150.30 (^{13}C), 141.15 (^{15}C), 135.29 (^1C), 135.01 (^{21}C), 134.54 (^{22}C), 129.25 (^{18}C), 129.15 ($^{16,20}\text{C}$), 126.26 (^3C), 125.51 (^{26}C), 124.10 ($^{17,19}\text{C}$), 123.50 (^{27}C), 121.35 (^4C), 120.16 (^{11}C), 115.42 (^{23}C), 109.32 (^{25}C), 45.17 (^6C), 39.52 (^8C), 32.10 (^7C). HRMS (ESI, m/z) calcd. for $\text{C}_{22}\text{H}_{19}\text{FN}_4\text{OS}$, 406.13; found 406.12465.

(2Z, 5Z)-3-(3-(1H-imidazol-1-yl)propyl)-5-(3-chlorobenzylidene)-2-(phenylimino)thiazolidin-4-one (S2A5): Color: Light brown. Yield: 68%. M.p.: 391-394 °C. FT-IR (KBr, ν , cm^{-1}): 1150 (C-F). ^1H NMR (500 MHz, $\text{DMSO}-d_6$, δ , ppm): 7.65 (s, 1H, ^1CH), 7.50 (s, 1H, ^{21}CH), 7.34 (d, 1H, ^4CH , $J = 7.10$ Hz), 7.25-6.95 (m, 9H, Ar-H), 6.90 (d, 1H, ^3CH , $J = 7.25$ Hz), 4.25 (t, 2H, $^6\text{CH}_2$, $J = 6.50, 7.1$ Hz), 3.80 (s, 2H, $^8\text{CH}_2$), 2.26 (m, 2H, $^7\text{CH}_2$). ^{13}C NMR (125 MHz, $\text{DMSO}-d_6$, δ , ppm): 171.05 (^{10}C), 150.3 (^{13}C), 141.15 (^{15}C), 135.29 (^1C), 135.01 (^{21}C), 134.61 (^{22}C), 133.52 (^{24}C), 129.25 (^{18}C), 129.15 ($^{16,20}\text{C}$), 126.26 (^3C), 126.01 (^{26}C), 125.50 (^{27}C), 124.10 ($^{17,19}\text{C}$), 121.50 (^{23}C), 121.35 (^4C), 120.32 (^{25}C), 120.16 (^{11}C), 45.17 (^6C), 39.50 (^8C), 32.10 (^7C). HRMS (ESI, m/z) calcd. for $\text{C}_{22}\text{H}_{19}\text{ClN}_4\text{OS}$, 422.10; found 422.09276.

(2Z, 5Z)-3-(3-(1H-imidazol-1-yl)propyl)-5-(3-methylbenzylidene)-2-(phenylimino)thiazolidin-4-one (S2A6): Color: Light brown. Yield: 65%. M.p.: 385-388 °C. FT-IR (KBr, ν , cm^{-1}): 1040

(C-Cl). ¹H NMR (500 MHz, DMSO-*d*₆, δ, ppm): 7.65 (s, 1H, ¹CH), 7.26 (s, 1H, ²¹CH), 7.25 (d, 1H, ⁴CH, *J* = 7.10 Hz), 7.10-6.95 (m, 9H, Ar-H), 6.90 (d, 1H, ³CH, *J* = 7.25 Hz), 4.25 (t, 2H, ⁶CH₂, *J* = 6.50, 7.1 Hz), 3.80 (s, 2H, ⁸CH₂), 2.29 (s, 3H, CH₃), 2.26 (m, 2H, ⁷CH₂). ¹³C NMR (125 MHz, DMSO-*d*₆, δ, ppm): 171.05 (¹⁰C), 150.32 (¹³C), 141.15 (¹⁵C), 136.50 (²⁴C), 135.29 (¹C), 135.01 (²¹C), 134.51 (²²C), 129.25 (¹⁸C), 129.15 (^{16,20}C), 126.26 (³C), 124.91 (²⁷C), 124.54 (²³C), 124.30 (²⁶C), 124.10 (^{17,19}C), 121.35 (⁴C), 121.22 (²⁵C), 120.16 (¹¹C), 45.17 (⁶C), 39.50 (⁸C), 35 (CH₃), 32.10 (⁷C). HRMS (ESI, *m/z*) calcd. for C₂₃H₂₂N₄O₅, 402.15; found 402.14567.

(2*Z*, 5*Z*)-3-(3-(1*H*-imidazol-1-yl)propyl)-5-(3-nitrobenzylidene)-2-(phenylimino)thiazolidin-4-one (**S2A7**): Color: Light brown. Yield: 72%. M.p.: 382-385 °C. FT-IR (KBr, ν, cm⁻¹): 1020 (C-Cl). ¹H NMR (500 MHz, DMSO-*d*₆, δ, ppm): 8.12 (s, 1H, ¹CH), 7.70 (d, 1H, ⁴CH, *J* = 7.10 Hz), 8.25 (s, 1H, ²¹CH), 7.25-6.95 (m, 9H, Ar-H), 6.90 (d, 1H, ³CH, *J* = 7.25 Hz), 4.25 (t, 2H, ⁶CH₂, *J* = 6.50, 7.1 Hz), 3.80 (s, 2H, ⁸CH₂), 2.26 (m, 2H, ⁷CH₂). ¹³C NMR (125 MHz, DMSO-*d*₆, δ, ppm): 171.05 (¹⁰C), 150.30 (¹³C), 146.50 (²⁴C), 141.15 (¹⁵C), 135.29 (¹C), 135.01 (²¹C), 134.52 (²⁷C), 134.52 (²²C), 129.25 (¹⁸C), 129.15 (^{16,20}C), 126.26 (³C), 125.50 (²⁶C), 124.10 (^{17,19}C), 121.35 (⁴C), 120.16 (¹¹C), 120.01 (²⁵C), 119.54 (²³C), 45.17 (⁶C), 39.51 (⁸C), 32.10 (⁷C). HRMS (ESI, *m/z*) calcd. for C₂₂H₁₉N₅O₃S 433.12; found 433.12531.

(2*Z*, 5*Z*)-3-(3-(1*H*-imidazol-1-yl)propyl)-5-(3-methoxybenzylidene)-2-(phenylimino)thiazolidin-4-one (**S2A8**): Color: Light brown. Yield: 70%. M.p.: 415-418 °C. FT-IR (KBr, ν, cm⁻¹): 1522 (N=O). ¹H NMR (500 MHz, DMSO-*d*₆, δ, ppm): 7.65 (s, 1H, ¹CH), 7.25 (s, 1H, ²¹CH), 7.34 (d, 1H, ⁴CH, *J* = 7.10 Hz), 7.15-6.95 (m, 9H, Ar-H), 6.90 (d, 1H, ³CH, *J* = 7.25 Hz), 4.25 (t, 2H, ⁶CH₂, *J* = 6.50, 7.1 Hz), 3.80 (s, 2H, ⁸CH₂), 2.26 (m, 2H, ⁷CH₂), 3.75 (s, 3H, OCH₃). ¹³C NMR (125 MHz, DMSO-*d*₆, δ, ppm): 171.05 (¹⁰C), 162.20 (²⁴C), 150.30 (¹³C), 141.15 (¹⁵C), 135.01 (²¹C), 135.29 (¹C), 134.50 (²²C), 129.25 (¹⁸C), 129.15 (^{16,20}C), 126.26 (³C), 125.40 (²⁶C), 124.10 (^{17,19}C), 121.35 (⁴C), 120.16 (¹¹C), 119.50 (²⁷C), 115.51 (²³C), 115.41 (²⁵C), 59 (OCH₃), 45.17 (⁶C), 39.52 (⁸C), 32.10 (⁷C). HRMS (ESI, *m/z*) calcd. for C₂₃H₂₂N₄O₂S 418.15; found 418.16478.

(2*Z*, 5*Z*)-3-(3-(1*H*-imidazol-1-yl)propyl)-5-(4-fluorobenzylidene)-2-(phenylimino)thiazolidin-4-one (**S2A9**): Color: Light brown. Yield: 69%. M.p.: 427-430 °C. FT-IR (KBr, ν, cm⁻¹): 1152 (C-F). ¹H NMR (500 MHz, DMSO-*d*₆, δ, ppm): 7.65 (s, 1H, ¹CH), 7.59 (s, 1H, ²¹CH), 7.45 (d, 1H, ⁴CH, *J* = 7.10 Hz), 7.25-6.95 (m, 9H, Ar-H), 6.90 (d, 1H, ³CH, *J* = 7.25 Hz), 4.25 (t, 2H, ⁶CH₂, *J* = 6.50, 7.1 Hz), 3.80 (s, 2H, ⁸CH₂), 2.26 (m, 2H, ⁷CH₂). ¹³C NMR (125 MHz, DMSO-*d*₆, δ, ppm): 171.05 (¹⁰C), 165.05 (²⁵C), 150.30 (¹³C), 141.15 (¹⁵C), 135.29 (¹C), 134.01 (²¹C), 131.50 (²²C), 130.2 (^{23,27}C), 129.25 (¹⁸C), 129.15 (^{16,20}C), 126.26 (³C), 124.10 (^{17,19}C), 121.35 (⁴C), 119.07 (¹¹C), 117.5 (^{24,26}C), 45.17 (⁶C), 39.51 (⁸C), 32.10 (⁷C). HRMS (ESI, *m/z*) calcd. for C₂₂H₁₉FN₄O₅ 406.13; found 406.13456.

(2*Z*, 5*Z*)-3-(3-(1*H*-imidazol-1-yl)propyl)-5-(4-chlorobenzylidene)-2-(phenylimino)thiazolidin-4-one (**S2A10**): Color: Light brown. Yield: 75%. M.p.: 377-380 °C. FT-IR (KBr, ν, cm⁻¹): 1025 (C-Cl). ¹H NMR (500 MHz, DMSO-*d*₆, δ, ppm): 7.65 (s, 1H, ¹CH), 7.47 (s, 1H, ²¹CH), 7.30 (d, 1H, ⁴CH, *J* = 7.10 Hz), 7.25-6.95 (m, 9H, Ar-H), 6.90 (d, 1H, ³CH, *J* = 7.25 Hz), 4.25 (t, 2H, ⁶CH₂, *J* = 6.50, 7.1 Hz), 3.80 (s, 2H, ⁸CH₂), 2.26 (m, 2H, ⁷CH₂). ¹³C NMR (125 MHz, DMSO-*d*₆, δ, ppm): 171.05 (¹⁰C), 150.30 (¹³C), 141.15 (¹⁵C), 135.29 (¹C), 135.02 (²⁵C), 134.01 (²¹C), 132.54 (²²C), 129.50 (^{24,26}C), 129.25 (¹⁸C), 129.15 (^{16,20}C), 128.72 (^{23,27}C), 126.26 (³C), 124.10 (^{17,19}C), 121.35 (⁴C), 119.07 (¹¹C), 45.17 (⁶C), 39.50 (⁸C), 32.10 (⁷C). HRMS (ESI, *m/z*) calcd. for C₂₂H₁₉ClN₄O₅ 422.10; found 422.10576.

(2*Z*, 5*Z*)-3-(3-(1*H*-imidazol-1-yl)propyl)-5-(4-methylbenzylidene)-2-(phenylimino)thiazolidin-4-one (**S2A11**): Color: Light brown. Yield: 65%. M.p.: 372-375 °C. FT-IR (KBr, ν, cm⁻¹): 2950 (C-H). ¹H NMR (500 MHz, DMSO-*d*₆, δ, ppm): 7.65 (s, 1H, ¹CH), 7.50 (d, 1H, ⁴CH, *J* = 7.10 Hz), 7.35-6.95 (m, 9H, Ar-H), 6.90 (d,

1H, ³CH, *J* = 7.25 Hz), 4.25 (t, 2H, ⁶CH₂, *J* = 6.50, 7.1 Hz), 3.80 (s, 2H, ⁸CH₂), 2.26 (m, 2H, ⁷CH₂), 2.42 (s, 3H, CH₃). ¹³C NMR (125 MHz, DMSO-*d*₆, δ, ppm): 171.05 (¹⁰C), 150.30 (¹³C), 141.15 (¹⁵C), 139.54 (²⁵C), 135.29 (¹C), 134.01 (²¹C), 131.24 (²²C), 129.25 (¹⁸C), 129.20 (^{24,26}C), 129.15 (^{16,20}C), 127.31 (^{23,27}C), 126.26 (³C), 124.10 (^{17,19}C), 121.35 (⁴C), 119.07 (¹¹C), 45.17 (⁶C), 39.51 (⁸C), 38.50 (CH₃), 32.10 (⁷C). HRMS (ESI, *m/z*) calcd. for C₂₃H₂₂N₄O₅ 402.15; found 402.51256.

(2*Z*, 5*Z*)-3-(3-(1*H*-imidazol-1-yl)propyl)-5-(4-nitrobenzylidene)-2-(phenylimino)thiazolidin-4-one (**S2A12**): Color: Light brown. Yield: 75%. M.p.: 392-395 °C. FT-IR (KBr, ν, cm⁻¹): 1525 (N=O). ¹H NMR (500 MHz, DMSO-*d*₆, δ, ppm): 8.27 (s, 1H, ²¹CH), 7.65 (s, 1H, ¹CH), 7.47 (d, 1H, ⁴CH, *J* = 7.10 Hz), 7.25-6.95 (m, 9H, Ar-H), 6.90 (d, 1H, ³CH, *J* = 7.25 Hz), 4.25 (t, 2H, ⁶CH₂, *J* = 6.50, 7.1 Hz), 3.80 (s, 2H, ⁸CH₂), 2.26 (m, 2H, ⁷CH₂). ¹³C NMR (125 MHz, DMSO-*d*₆, δ, ppm): 171.05 (¹⁰C), 150.30 (¹³C), 147.52 (²⁵C), 141.15 (¹⁵C), 140.54 (²²C), 135.29 (¹C), 134.01 (²¹C), 129.25 (¹⁸C), 129.21 (^{23,27}C), 129.15 (^{16,20}C), 126.50 (^{24,26}C), 126.26 (³C), 124.10 (^{17,19}C), 121.35 (⁴C), 119.07 (¹¹C), 45.17 (⁶C), 39.55 (⁸C), 32.10 (⁷C). HRMS (ESI, *m/z*) calcd. for C₂₂H₁₉N₅O₃S 433.12; found 433.14576.

(2*Z*, 5*Z*)-3-(3-(1*H*-imidazol-1-yl)propyl)-5-(4-methoxybenzylidene)-2-(phenylimino)thiazolidin-4-one (**S2A13**): Color: Light brown. Yield: 65%. M.p.: 402-405 °C. FT-IR (KBr, ν, cm⁻¹): 1160 (C-O). ¹H NMR (500 MHz, DMSO-*d*₆, δ, ppm): 7.65 (s, 1H, ¹CH), 7.59 (s, 1H, ²¹CH), 7.51 (d, 1H, ⁴CH, *J* = 7.10 Hz), 7.25-6.95 (m, 9H, Ar-H), 6.90 (d, 1H, ³CH, *J* = 7.25 Hz), 4.25 (t, 2H, ⁶CH₂, *J* = 6.50, 7.1 Hz), 3.85 (s, 2H, ⁸CH₂), 3.79 (s, 3H, OCH₃), 2.26 (m, 2H, ⁷CH₂). ¹³C NMR (125 MHz, DMSO-*d*₆, δ, ppm): 171.05 (¹⁰C), 162.53 (²⁵C), 150.30 (¹³C), 141.15 (¹⁵C), 135.29 (¹C), 134.01 (²¹C), 129.25 (¹⁸C), 129.15 (^{16,20}C), 128.51 (^{23,27}C), 126.31 (²²C), 126.26 (³C), 124.10 (^{17,19}C), 121.35 (⁴C), 119.07 (¹¹C), 112.16 (^{24,26}C), 57.12 (OCH₃) 45.17 (⁶C), 39.50 (⁸C), 32.10 (⁷C). HRMS (ESI, *m/z*) calcd. for C₂₃H₂₂N₄O₂S 418.15; found 418.15456.

2.3. In vitro antimicrobial activity

Disk diffusion susceptibility method [25] in accordance with National Committee for Clinical Laboratory Standards (NCCLS) guidelines was employed to investigate antibacterial activity of the compounds against Gram positive (*B. subtilis*, MTCC No 10619 and *S. aureus* MTCC No 96), and Gram-negative bacteria (*P. aeruginosa*, MTCC No 1748 and *E. coli*, MTCC No 68). Pure microbial strains were obtained from MTCC IMTECH, Chandigarh, India. Mueller-Hinton agar (HiMedia) was melted and subsequently poured (20 mL) into Petri plates (100 mm) and kept undisturbed at room temperature to solidify. A representative sample of the media was kept at 37 °C in BOD incubator for 24 hours to check the sterility. The culture of each bacterium in saline was uniformly spread over the media with a cotton swab. Sterile filter paper discs of 6 mm diameter (HiMedia) impregnated with respective concentrations of compounds in DMSO was applied to the surface of inoculated plates. The plates were kept in BOD incubator for 24 hrs at 37 °C and subsequently examined for bacterial growth. The results are expressed as zone of inhibition in millimeters (mm). Experiments were done in triplicate and on average standard deviation of < 0.5 was observed.

Agar dilution method [26] was used to calculate the MIC (minimum inhibitory concentration) of synthesized molecules. The pure bacterial strains were streaked onto nutrient-rich (Mueller-Hinton) agar plates to obtain single colonies. The plates were incubated at 37 °C for 22 hours. For each strain, four morphologically similar colonies were selected and transferred with a cotton swab into sterile capped glass tube containing sterile saline solution. Inoculum size for each test strain was adjusted to 10⁴ CFU/mL (Colony Forming Unit per milliliter) with sterile saline through turbidimetric method.

Table 1. Molinspiration and Molsoft prediction of molecular total polar surface area (TPSA), drug score, number of rotatable bonds (n_{rotb}), solubility (log s) and Lipinski parameters.

Compound	TPSA	Drug score	n_{rotb}	Log s	Log P	MW	HBA	HBA	Lipinski violations
S2A3	52.20	-0.30	6	-4.61	3.92	388.14	5	0	0
S2A4	52.20	-0.22	6	-4.92	4.18	406.12	5	0	0
S2A5	52.20	-0.14	6	-5.50	4.63	422.92	5	0	0
S2A6	52.20	-0.22	6	-4.93	4.32	402.14	5	0	0
S2A7	98.02	-0.39	7	-5.03	3.51	433.12	8	0	0
S2A8	61.43	-0.29	7	-4.75	3.92	418.16	6	0	0
S2A9	52.20	0.01	6	-5.13	4.18	406.13	5	0	0
S2A10	52.20	0.18	6	-5.57	4.63	422.10	5	0	0
S2A11	52.20	-0.33	6	-5.07	4.32	402.51	5	0	0
S2A12	98.02	-0.45	7	-5.11	3.51	433.14	8	0	0
S2A13	61.43	-0.30	7	-4.61	3.92	418.15	6	0	0

Stock solution of 1000 $\mu\text{g/mL}$ for each compound was prepared in 1% DMSO. The stock solutions were further diluted with saline to get solutions of concentrations 500 to 2.4 $\mu\text{g/mL}$. 1 mL each of the test solution and bacterial inoculum (10^4 CFU/mL) were mixed with nutrient agar and poured in Petri plates. The plates were incubated at 37 °C for 24 hrs. MIC was defined as the lowest concentration of tested compound which prevented the visible growth of bacteria.

2.4. *In silico studies and molecular docking simulations*

Molecular properties for the synthesized compounds were calculated by Molinspiration [27] and Molsoft [28] web servers. Before docking the compounds were optimized at B3LYP/ 6-31G(d,p) level using Gaussian G09 software [29]. Docking simulations were carried using Autodock Vina Software, employing the standard protocol [30]. The crystal structures of multiple DNA strands used in docking were downloaded from the Protein data bank (PDB) database.

3. Results and discussion

3.1. Spectral analysis

The formation of compound S2A1 was confirmed by recording its FT-IR, ^1H NMR, ^{13}C NMR and HRMS spectra. Presence of N-H stretching vibrations at 3390 and 3273 cm^{-1} confirms the formation of thiourea. Shifts in aromatic C-H stretch (3063 cm^{-1}) and disappearance of primary amine vibrations corroborated the above results. ^1H NMR spectra of this compound showed two broad singlets which were interpreted for thiourea N-H at δ 7.7 and 9.5 ppm. The most prominent peaks in ^{13}C NMR spectra at δ 180.0 ppm confirmed the presence of C=S linkage. The molecular ion peak ($[\text{M}]^+ = 260.35351$ m/z) corresponds to the molecular mass of the compound.

The formation of compound S2A2 was similarly confirmed from the corresponding spectra. FT-IR spectra shows a sharp band at 1730 cm^{-1} which was assigned to carbonyl C=O stretch. Disappearance of N-H and C=S stretching vibrations and presence of N=C and N-C-S ring vibrations at 1570 and 1269 cm^{-1} confirmed the formation of thiazolidinone ring. ^{13}C NMR spectra shows peaks for carbonyl and methylene carbons at δ 180 and 30 ppm, respectively, which is consistent with formation of thiazolidinone ring. The molecular ion peak ($[\text{M}]^+ = 300.17456$ m/z) corresponds to the molecular mass of the compound.

The final compounds S2A3-13 were similarly characterized by recording the FT-IR, ^1H NMR and ^{13}C NMR spectra of the compounds. The absorption band at 1680 cm^{-1} in FT-IR spectra corresponds to arylidene C=C stretch. A singlet at δ 6.9-7.2 ppm and a multiplet at δ 6.9-8.1 ppm corresponding to CH and aromatic protons, respectively, confirm the formation of the subsequent compounds. The substitution pattern in the phenyl ring was confirmed from the splitting pattern and

corresponding coupling constants in the aromatic region of NMR spectra.

3.2. *In silico study of drug likeness and molecular properties*

As a starting point to evaluate the pharmaceutical potential of the synthesized molecules we decided to calculate some *in silico* properties for these molecules. Most of the clinical drugs available in market possess some peculiar properties and it has been possible to numerically distinguish such properties (descriptors). A drug candidate should have certain structural features which could increase its bioavailability and help it cross the blood brain barrier. It has become possible to quantify such structural features in terms of molecular properties like "Rule of 5", Molecular Polar Surface Area (TPSA), Molecular Volume, Number of Rotatable Bonds (n_{rotb}) etc. The Lipinski "Rule of Five" [31] highlights the importance of physical parameters like lipophilicity ($\log P \leq 5$), molecular weight (≤ 500) and the number of hydrogen bond donors (≤ 10)/ acceptors (≤ 10) for bioavailability and oral absorption. TPSA descriptor characterizes drug absorption, intestinal absorption, bioavailability, Caco-2 permeability and blood-brain barrier penetration [32]. n_{rotb} topological parameter is a measure of molecular flexibility which is directly related to oral bioavailability [33]. It is evident from Table 1 that all the synthesized molecules follow Lipinski rule of five. The nitro derivatives have the highest polar surface area in addition to HBA, indicating that they can participate in donor-acceptor interactions. Fluoro and chloro derivatives are predicted as good drug molecules based on drug score. Halogens particularly fluorine and chlorine positively influence the biological properties of molecules. "Halogen bonding" has been found to be one of the factors by which chlorine alters the biological effect of molecules [34]. From these studies it was found that the molecules possess drug like properties and can interact with biomolecules to exert a particular effect. Having satisfied ourselves with primary *in silico* screening assay of these compounds we decided to carry *in vitro* antimicrobial activity of these compounds to further investigate their biological potential.

3.3. *In vitro antimicrobial activity*

The structure of a molecule would always decide what type of activity a molecule may possess. A look at the current literature reveals that molecules possessing similar structural features as we reported here have been found to be highly active against various pathogenic bacteria and certain types of cancers [14]. Based on this chemical institution, we decided to probe antimicrobial potency of the synthesized molecules. Disc diffusion and agar dilution susceptibility tests were used to probe antimicrobial activity.

Table 2. MIC values in $\mu\text{g/mL}$ for the synthesized molecules calculated by agar dilution method. All values are presented as mean of three experiments $\pm\text{SD}=\text{Standard deviation (n=3)}$.

Compound	Minimum inhibitory concentration (MIC) against bacteria in $\mu\text{g/mL} \pm\text{SD}$			
	<i>S. aureus</i> (MTCC 96)	<i>B. subtilis</i> (MTCC 10619)	<i>E. coli</i> (MTCC 68)	<i>P. aeruginosa</i> (MTCC 1748)
S2A3	12.5 \pm 0.23	25 \pm 0.43	25 \pm 0.34	25 \pm 0.13
S2A4	3.125 \pm 0.23	12.5 \pm 0.34	25 \pm 0.45	6.25 \pm 0.34
S2A5	6.25 \pm 0.34	6.25 \pm 0.34	3.125 \pm 0.66	3.125 \pm 0.23
S2A6	25 \pm 0.45	25 \pm 0.23	12.5 \pm 0.76	25 \pm 0.34
S2A7	3.125 \pm 0.56	2.0 \pm 0.45	2.0 \pm 0.55	6.25 \pm 0.45
S2A8	12.5 \pm 0.45	25 \pm 0.45	25 \pm 0.56	25 \pm 0.24
S2A9	25 \pm 0.45	12.5 \pm 0.56	25 \pm 0.23	12.5 \pm 0.65
S2A10	12.5 \pm 0.34	25 \pm 0.56	6.25 \pm 0.34	6.25 \pm 0.34
S2A11	25 \pm 0.12	25 \pm 0.23	50 \pm 0.45	50 \pm 0.46
S2A12	12.5 \pm 0.15	12.5 \pm 0.23	3.25 \pm 0.34	6.25 \pm 0.75
S2A13	25 \pm 0.3	25 \pm 0.45	12.5 \pm 0.12	25 \pm 0.23
Ciprofloxacin	3.125 \pm 0.82	6.25 \pm 0.24	3.125 \pm 0.4	3.125 \pm 0.42
Streptomycin	6.25 \pm 0.62	3.125 \pm 0.2	6.25 \pm 0.6	3.125 \pm 0.42

After obtaining encouraging results from primary screening of synthesized molecules against selected microbial strains with disc diffusion method, the MIC values were calculated with agar dilution method. As is evident from Table 2, most of the compounds inhibit the growth of both Gram positive and Gram-negative bacterial strains to substantial levels. A careful observation of MIC values shows compound S2A7 to be most active molecule with highest potency against *B. subtilis* and *E. coli* with MIC value 2.0 $\mu\text{g/mL}$ which is higher than the standard drugs Streptomycin and Ciprofloxacin. S2A5 is highly active against *P. aeruginosa* and *E. coli*. S2A4 and S2A12 show high activity against *S. aureus* and *E. coli*, respectively. A close look at the structure activity relationships shows that nitro group when present at meta position complements the activity. Amongst the para-substituted compounds para-nitro derivative was found to be most potent. The higher activity of nitro derivatives could be due to the fact that nitro group contributes hydrogen bonding atoms which manifest lipophilic properties of the molecule thus resulting in stronger substrate-inhibitor interactions. Both nitro and methoxy groups contribute H-bonding atoms and oxygen in particular increases the hydrophilic character of the molecule which in turn increases oral absorption. Halogens in general and chlorine in particular increase the oral absorption and potency of a drug candidate [34]. Under this scenario compound S2A5 is expected to have good oral absorption and therefore high bioavailability. As compound S2A7 was found to possess broad spectrum activity and was highly active against all the bacterial strains, we decided to probe DNA as a possible target for this molecule.

3.4. DNA-binding study

3.4.1. UV-Vis spectroscopy

The susceptibility tests revealed that the synthesized molecules inhibit growth and multiplication of the bacteria. Amongst the various microbial targets DNA being an established target for many commercial antimicrobial drugs, was probed as target for the synthesized molecules. UV-Visible absorption spectroscopy is a useful technique to probe drug-DNA binding [35]. The change in absorption intensity and λ_{max} due to changes in conformation and structure of DNA upon interaction with inhibitor characterizes the type of interaction involved. The magnitude of these changes reflects the strength of interaction. Intercalative binding produces hypochromism with red shift which is believed to happen due to interaction between π antibonding orbital (π^*) of intercalated molecule and π -bonding orbital (π) of DNA base pairs [23]. Electrostatic interaction results in hyperchromism for both DNA and interacting molecule, which reflects conformational change. Groove binding results in hyperchromism with no or very little

red shift, which is believed to be due to interaction between electronic states of interacting molecules and nitrogenous bases of DNA [36]. The characteristic absorption peak of DNA at 260 nm (due to π - π transition of base pairs of sm-DNA) was taken as reference to study the interaction. UV-Vis spectra of sm-DNA with increasing concentrations of S2A7 is shown in Figure 3. As is evident from the spectra, with increasing concentration of S2A7, the absorbance of both DNA and DNA-Etbr complex at 260 nm increases (hyperchromism) with no red shift. This indicates S2A7 interacts with DNA and the possible mode of interaction could be groove binding or electrostatic interaction. To further distinguish the type of interaction, fluorescence quenching titrations were carried with compound S2A7.

3.4.2. Fluorescence spectroscopy

Fluorescence emission spectroscopy is used to probe binding mode in drug-DNA interactions [37]. Quenching of fluorescence provides valuable information about the interaction of quencher and fluorophore. Fluorescence emission spectrum of S2A7 shows emission maxima at 362 nm when excited with 290 nm light. As shown in Figure 4a subsequent addition of sm-DNA to S2A7 results in quenching of fluorescence with a very slight change in emission maxima. This shows that S2A7 binds with DNA and rules out the possibility of intercalative binding. This also suggests that S2A7 interacts with DNA through groove binding. Stern-Volmer Equation (1) was used to study quenching process and to calculate quenching constant.

$$F_0/F = 1 + K_q\tau_0 [Q] = 1 + K_{sv} [Q] \quad (1)$$

where τ_0 is the average life expectancy of fluorescent molecule, F_0 and F , respectively, represent fluorescence intensities of S2A7 in absence and presence of sm-DNA. K_q denotes quenching rate constant and K_{sv} represents Stern-Volmer quenching constant which is a measure of efficiency of fluorescence quenching by DNA.

As is evident from Figure 4a plot of F_0/F (fluorescence quenching) versus concentration of sm-DNA shows a linear relationship. The slope of this curve 1.3279×10^5 gives K_{sv} which is in the range of typical groove binders [38]. The fluorescence lifetime for a macromolecule in general is approximately 10^{-8} seconds. Substituting this value in Equation (1), the quenching constant K_q was found to be 1.3279×10^{13} L/mol.s. This value is much larger than the biggest diffusion control collision constant between a small molecule and a macromolecule (2×10^{10} L/mol.s). Therefore, the only possible quenching mode operative in present case is believed to be Static quenching.

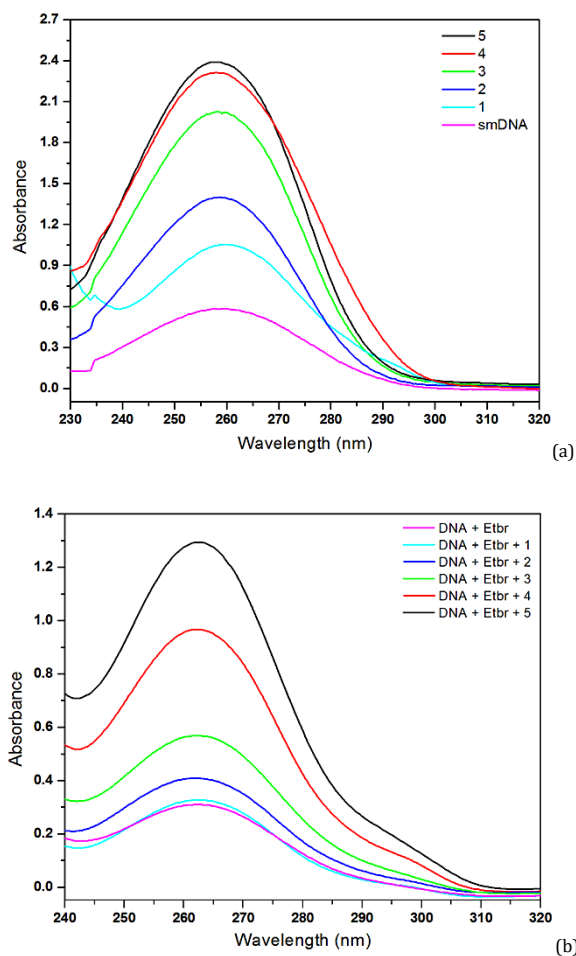


Figure 3. Interaction of compound S2A7 with sm-DNA using absorption spectroscopy. Absorption spectra of DNA in the absence (a) and presence (b) of ethidium bromide (Etbr) with increasing concentration of S2A7.

Modified Stern-Volmer Equation (2) was used to calculate binding sites 'n' and binding constant 'K_A' [39].

$$\text{Log} [(F_0 - F)/F] = \text{Log } K_A + n \times \text{Log } C \quad (2)$$

As is evident from Figure 4b the value of K_A and n were found to be 0.1287 × 10² L/mol and 1.43, respectively. The value for K_A is much smaller than that found for intercalative mode [40], groove binding seems to be operating in the binding of S2A7 to sm-DNA.

3.4.3. Competitive study

Etbr is a classic DNA intercalator which produces strong fluorescence on intercalation with DNA. Etbr was used to probe intercalative mode of the compound S2A7. Figure 4b shows the fluorescence spectra of DNA in complex with intercalator Etbr. On addition of S2A7 the fluorescence intensity of DNA-Etbr complex doesn't change much. Thus, S2A7 is not an effective quencher which indicates that compound S2A7 doesn't compete with Etbr as intercalator. Hence, forth the possibility of S2A7 as DNA-intercalator doesn't hold.

3.4.4. Gel electrophoresis

The mobility of DNA on agarose gel depends on its size, charge and flexibility. Therefore, DNA with bound molecules because of higher molecular weight would migrate slower as compared to one which doesn't bind with drug molecule. DNA-

Etbr in complex with compound S2A7 travels smaller distance as compared to Etbr-DNA complex (Figure 5). Due to increase in the molecular weight of the complex its mobility is affected which ultimately renders its migration on agarose gel. This is a direct evidence of S2A7 binding with DNA without competing with Etbr. The only binding mode possible is groove binding.

3.4.5. Docking studies

Molecular docking is an important tool in bioinformatics which predicts binding mode and affinity (docking score) of small molecules towards a particular target [41]. It has become possible with molecular docking to distinguish between groove binding and intercalation [42]. With the aim of validating the binding mode of S2A7, molecular docking simulations were carried on different DNA fragments with varying A/T content. Both intercalation and groove binding sites were targeted. Compound S2A7 binds at the minor groove of DNA without exception in all the docked DNA fragments. Crystal structure 1G3X co-crystallized with acridine-peptide drug and 1Z3F were employed to probe intercalative mode of S2A7. The grid dimensions were set to include the intercalation space. Both co-crystallized acridine-peptide drug and compound S2A7 were docked at intercalative binding site. The co-crystallized drug binds at the intercalative space in the same confirmation as present in X-ray crystal structure (Figure 6).

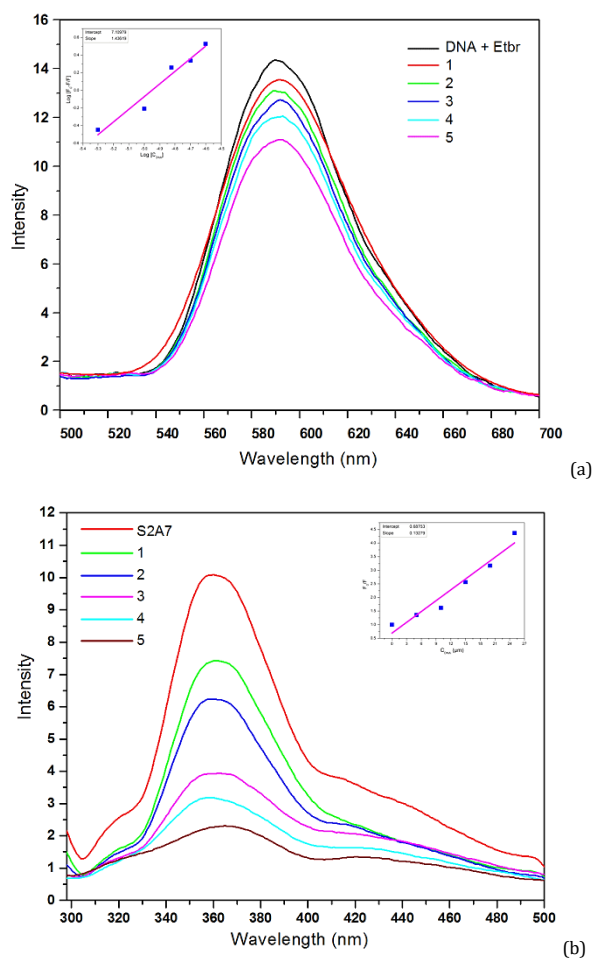


Figure 4. (a) Interaction of S2A7 with sm-DNA using fluorescence spectroscopy. Fluorescence emission spectra of S2A7 (5.5×10^{-3} mol/L) in presence of increasing concentrations of sm-DNA (0-50 μ M). Stern-Volmer plot for interaction of S2A7 with sm-DNA. Plot of $\log((F_0-F)/F)$ versus $\log C_{DNA}$. K_{SV} was calculated from the slope of plot F_0/F vs. DNA concentration. (b) Competitive displacement assays; Fluorescence spectra of DNA-EtBr complex with increasing concentration of S2A7.

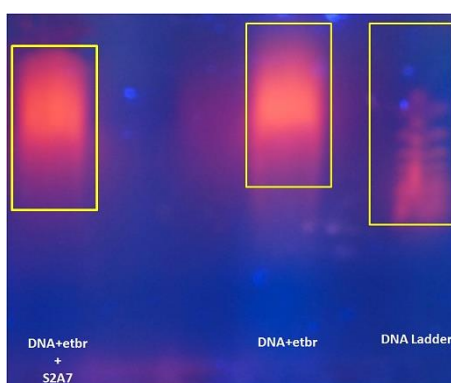


Figure 5. Gel electrophoresis image of S2A7 complexed with DNA and DNA with EtBr.

However, compound S2A7 binds only at the minor groove both in 1G3X and 1Z3F (Figure 7). With other DNA fragments the grid dimensions were set to include all the base pairs of DNA for docking, even then the molecule S2A7 specifically binds at the minor groove. Second interesting observation which is evident from Table 3 is that as the Adenine-Thiamine base pair content increases in the DNA fragments, the binding affinity of S2A7 towards DNA increases. This shows preferential affinity of S2A7 towards A-T base pairs.

As is evident from Figure 7, the docked molecules interact with DNA through non-covalent interactions mostly H-

bonding and van der Waals interactions. In case of 463D π - π T stacking interaction is found between π electron clouds of imidazole ring with pyrimidine ring of DG14 (Figure 8). The formation of multiple H-bonds is clear evidence in favor of strong ligand-DNA interaction. Docking scores in the range of -6.0 to -9.2 kcal/mol were predicted for S2A7 when docked with different fragments of DNA. From these results we conclude that the synthesized molecules have potential to bind at the minor groove of DNA and could exert antimicrobial as well as anti-cancer effect by interfering with the functioning of DNA.

Table 3. DNA sequences for DNA fragments and binding sites for BSA are shown. Binding affinity of S2A7 with these fragments is in units of kcal/mol. H-bond forming bases/residues are also shown.

PDB ID	Sequence (DNA) Binding site (BSA)	ΔG (kcal/mol)	H-bonding bases/residues	No of H-bonds	Grid dimensions
2ELG	(CGCGCG)2	-7.1	DG4, DG6, DG8, DG10	4	4.917, 0.628, 5.881
1K2K	(CGTACG)2	-7.7	DG8, DT9, DA10, DC5, DG2	5	0.256, 1.993, 7.420
463D	(CGCGAATTCGCG)2	-7.3	DG10 (DG14 π - π)	1	-7.257, 13.496, 1.221
1VTJ	(CGCGATATCGCG)2	-8.3	DA19	1	14.278, 22.413, 75.817
1BNA	(CGCGAATTCGCG)2	-8.6	DC9, DG10, DC11, DG14, DG16, DC15	6	12.833, 21.133, 8.694
121D	(CGCAAATTCGCG)2	-9.0	DT19	1	14.404, 22.479, 78.761
1G3X	(CGCGAATTCGCG)2	-9.2	DG610, DG616	2	59.860, 52.124, 59.663
1Z3F	(CGATCG)2	-6.5	DG2, DG2, DA3	3	0.86, 17.332, 37.318
3V03	IIIA	-7.2	Asp111, Leu112, Thr190	3	27.556, 22.974, 41.858
	IIA	-6.0	Glu207, Arg208	2	

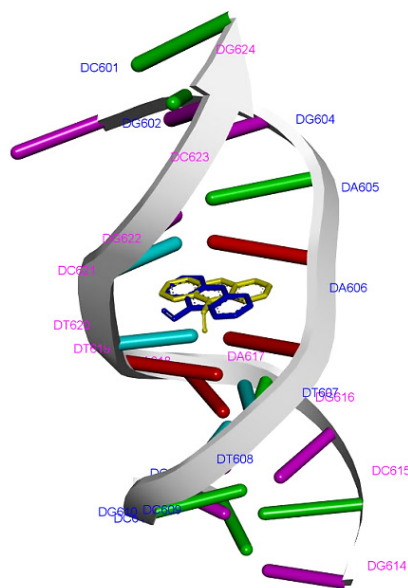


Figure 6. Superimposition of docked conformation (blue) over the co-crystallized conformation (yellow) of acridine-peptide drug shows RMSD value below 2Å, confirming the reliability of docking protocol.

3.5. BSA-binding study

3.5.1. UV-Vis spectroscopy

UV-Visible spectra of BSA shows absorption band at 210 and 300nm. As is shown in Figure 9a, on addition of increasing concentrations of S2A7 the absorption intensity decreases. The change in the absorption intensity is probably due to the changes in framework conformations of BSA upon interaction with S2A7. These results show that S2A7 binds with BSA.

3.5.2. Fluorescence spectroscopy

Quenching of fluorescence provides valuable information about the interaction of quencher and fluorophore. Fluorescence emission spectrum of BSA shows emission maxima at 342 nm when excited with 280 nm light. This fluorescence is believed to be from the Tryptophan (Trp) residue in BSA [43]. As shown in Figure 9b subsequent addition of S2A7 to BSA results in quenching of fluorescence with no change in emission maxima. This suggests that there is a change in the microenvironment of Trp residues which can happen only if there is a binding interaction involving Trp residue. Thus, S2A7 binds with BSA and interacts with Trp residue which ultimately results in fluorescence quenching. Stern-Volmer equation was used to study quenching process and to calculate quenching constant. As is evident from Figure 9b plot of F_0/F versus concentration of sm-DNA shows a linear relationship. The slope of this curve 7.73×10^6 gives K_{sv} . On average the fluorescence lifetime for a macromolecule is approximately

10^{-8} seconds. Therefore, from Equation (1), the quenching constant K_q was found to be 7.73×10^{13} L.mol⁻¹s⁻¹. This value is much larger than the biggest diffusion control collision constant between a small molecule and a macromolecule (2×10^{10} L.mol⁻¹s⁻¹). Therefore, the only possible quenching mode operative in present case is believed to be Static quenching. Binding sites 'n' and binding constant 'K' calculated by employing Equation (2) were found to be 6.1×10^{-3} L.mol⁻¹ and 0.92, respectively. This indicates that for S2A7 would always bind at the IIIA binding site which was also confirmed by docking results. The large binding constant value indicates a strong interaction between S2A7 and BSA.

3.5.3. Docking studies

Serum albumin being the most abundant circulatory protein (60% of plasma) has many physiological functions and plays vital role in transport of drugs. For a drug molecule to have large bio-distribution it should have strong affinity towards serum albumin. As is well known that BSA has two well recognized binding sites one in subdomain III (IIIA) and another in subdomain II (IIA). It is clear from Figure 11 that S2A7 binds with BSA at both sites, however the comparative binding affinity at the sites varies. The change in free energy is more negative when S2A7 binds at the hydrophobic binding pocket in subdomain IIIA than IIA indicating that binding at IIIA is energetically more favorable. The binding affinity at both the sites and H-bonding residues are shown in Table 3. It is clear that S2A7 prefers binding in subdomain IIIA.

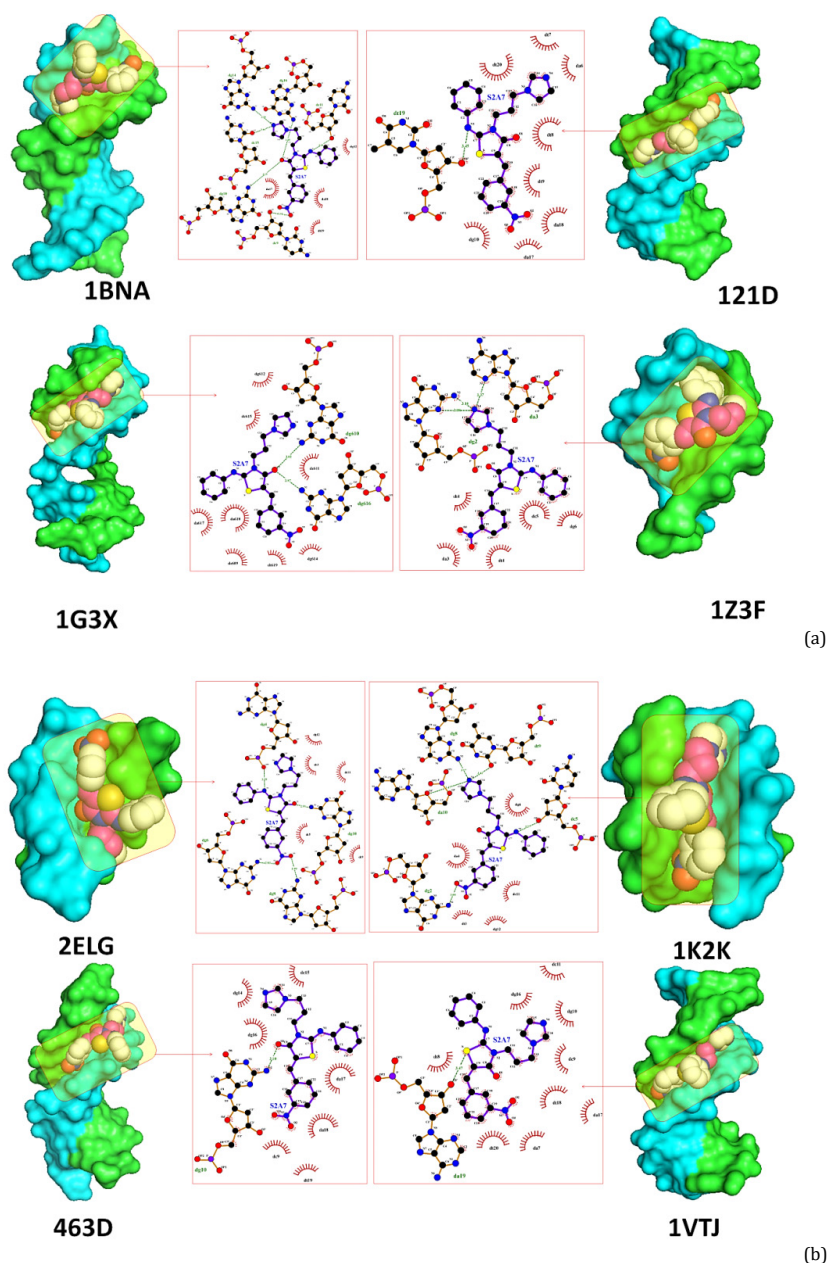


Figure 7. (a) Surface and schematic representation of DNA fragments shows that the docked molecule S2A7 (in ball representation) binds at the minor groove. In spite of an intercalation space in 1G3X, S2A7 specifically binds at the minor groove. (b) Schematic representation for the interactions of S2A7 with different DNA fragments. H-bonds are shown by green dotted lines. Nitrogenous bases represented by brown crescents are involved in hydrophobic interactions.

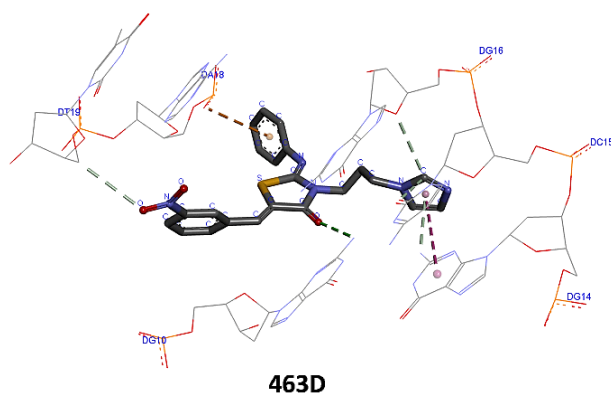


Figure 8. Detailed interactions of S2A7 with 463D, dotted lines represent the interactions. H bonds and π - π T interactions are represented by green and pink dotted lines, respectively.

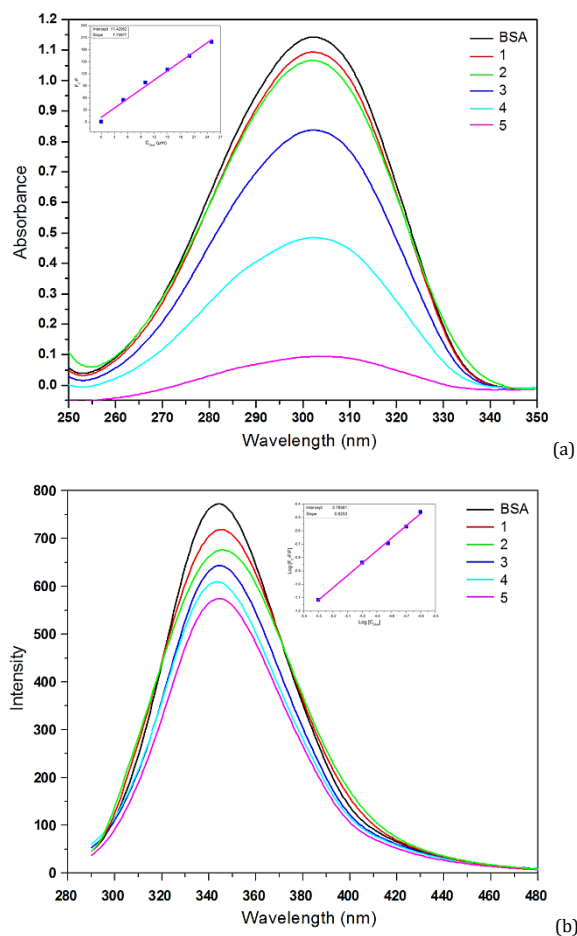


Figure 9. (a) Interaction of S2A7 with BSA using absorption spectroscopy. Stern-Volmer plot for interaction of S2A7 with BSA. K_{SV} was calculated from the slope of plot F_0/F vs. DNA concentration. (b) Fluorescence emission spectra of BSA in presence of increasing concentrations of S2A7 along with plot of $\log((F_0-F)/F)$ versus $\log C_{DNA}$.

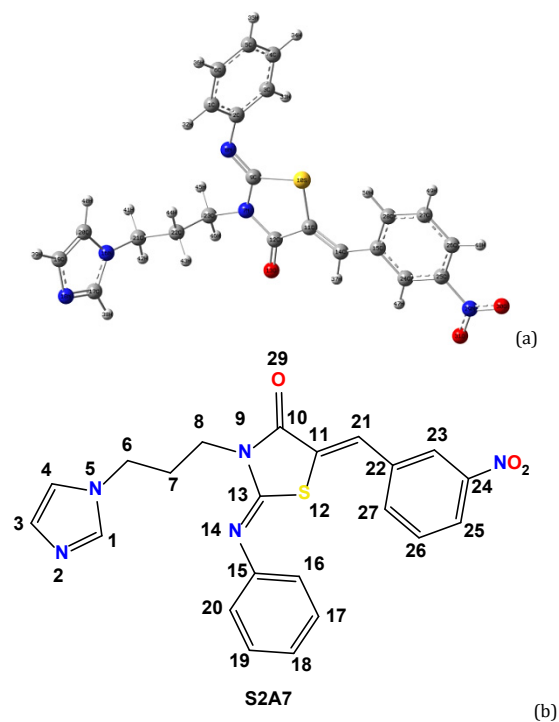


Figure 10. (a) B3LYP/6-31G(d,p) optimized geometry of S2A7 and (b) Structure of S2A7 with numbering for NMR interpretation.

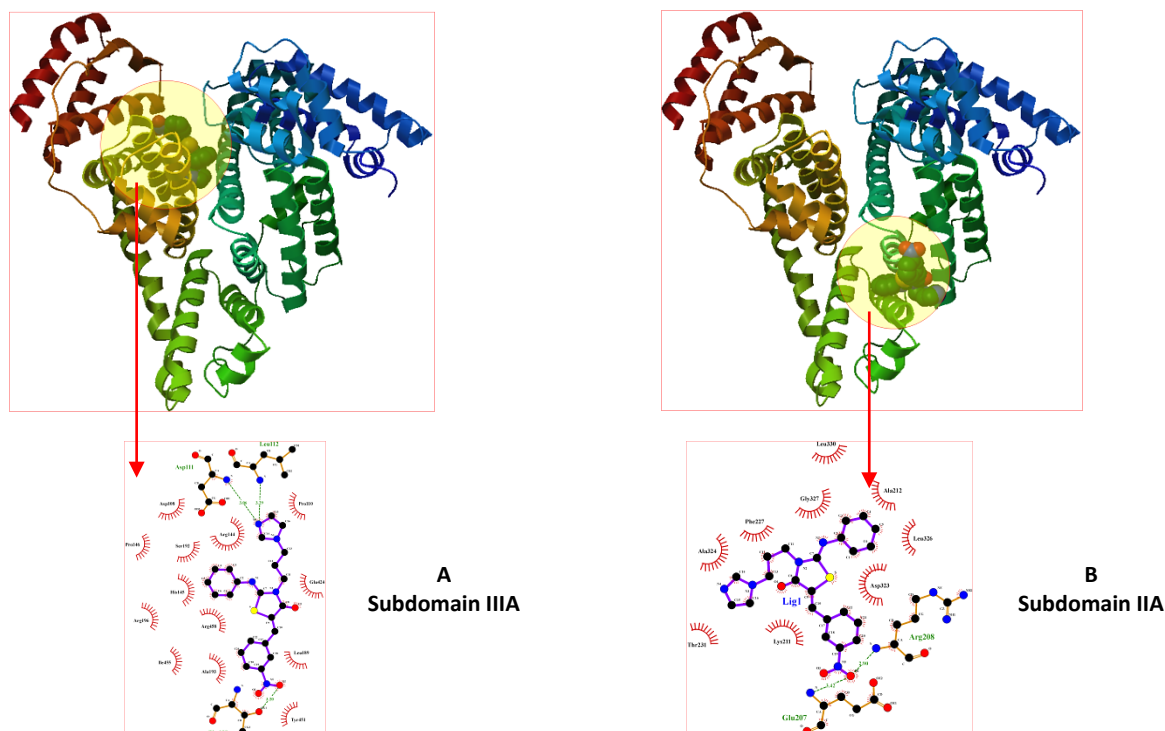


Figure 11. Interaction of S2A7 with BSA. S2A7 shows preferential binding at subdomain IIIA. Inspect (a) and (b) show interacting residues at subdomain IIIA and IIA.

4. Conclusion

In conclusion, we were successful in establishing the initial hypothesis of synthesizing broad-spectrum antibiotics through experimentation. As a starting point *in silico* molecular descriptor calculations predicted drug like properties in the synthesized molecules which were later confirmed by *in vitro* susceptibility tests against some gram positive and Gram-negative bacteria. Utilizing UV-Visible, fluorescence, gel electrophoresis and molecular docking techniques DNA was probed as drug target. It was found that the most potent molecule S2A7 binds at DNA minor groove and gets involved in Van der Waals, H-bonding and hydrophobic interactions. High binding affinity (-9.2 kcal/mol) and binding constant of 0.1287×10^2 L/mol were calculated for compound S2A7. Presence of nitro and chloro groups substantially increased the activity of molecules when present at *meta* position in the substituted phenyl ring. Both *in vitro* and *in silico* studies established that S2A7 has strong affinity towards serum albumin. This shows that the compound would have high bio-distribution. In conclusion the compounds we report have shown great promise for their antimicrobial potential. As they interact and bind with DNA, anti-cancer activity is also predicted for the synthesized molecules. Further structural optimization may lead to discovery of other leads for antimicrobial/anticancer drug discovery.

Acknowledgement

The authors would like to acknowledge Sophisticated Analytical Instrumentation Facility, Panjab University, Chandigarh and Central Instrumentation Laboratory (Dr. Harisingh Gour University Sagar, Madhya Pradesh), India for providing instrument facility. Javeed Ahmad War acknowledges financial support from Department of Science and Technology, New-Delhi, India under INSPIRE program (INSPIRE ID: IF120399). Assistance of Mr. Arun Kumar (Department of Zoology, Dr. Harisingh Gour University Sagar

and Madhya Pradesh) in carrying biological tests is highly acknowledged.

Disclosure statement

Conflict of interests: The authors declare that they have no conflict of interest.

Author contributions: Major contributions were from first author (Javeed Ahmad War).

Ethical approval: All ethical guidelines have been adhered.

Sample availability: Samples of the compounds are available from the author.

Funding

Department of Science and Technology, Ministry of Science and Technology, India.

<http://dx.doi.org/10.13039/501100001409>

ORCID

Javeed Ahmad War

<http://orcid.org/0000-0001-6652-2846>

Santosh Kumar Srivastava

<http://orcid.org/0000-0001-8237-9189>

References

- [1]. Hofer, U. *Nature Rev. Microbiol.* **2019**, *17*(1), 3-3.
- [2]. Van Boeckel, T. P.; Pires, J.; Silvester, R.; Zhao, C.; Song, J.; Criscuolo, N. G.; Gilbert, M.; Bonhoeffer, S.; Laxminarayan, R. *Science* **2019**, *365*(6459), 1-5.
- [3]. Karaiskos, I.; Lagou, S.; Pontikis, K.; Rapti, V.; Poulakou, G. *Front. Public Health* **2019**, *7*, 151, 1-25.
- [4]. Organization, W. H. Antimicrobial resistance: global report on surveillance. World Health Organization, ISBN: 978 92-4-156474-8, 2014.

- [5]. Dougan, G.; Dowson, C.; Overington, J.; Participants, N. G. A. D. S. *Drug Discov. Today* **2019**, *24*(2), 452-461.
- [6]. Chernov, V. M.; Chernova, O. A.; Mouzykantov, A. A.; Lopukhov, L. L.; Aminov, R. I. *Expert Opin. Drug Disc.* **2019**, *14*(5), 455-468.
- [7]. Desai, N.; Joshi, V.; Rajpara, K.; Makwana, A. H. *Arabian J. Chem.* **2017**, *10*, S589-S599.
- [8]. Obinata, D.; Ito, A.; Fujiwara, K.; Takayama, K. I.; Ashikari, D.; Murata, Y.; Yamaguchi, K.; Urano, T.; Fujimura, T.; Fukuda, N. *Cancer Sci.* **2014**, *105*(10), 1272-1278.
- [9]. Hu, Y.; Shen, Y.; Wu, X.; Tu, X.; Wang, G. X. *Eur. J. Med. Chem.* **2018**, *143*, 958-969.
- [10]. Devi, P. B.; Samala, G.; Sridevi, J. P.; Saxena, S.; Alvala, M.; Salina, E. G.; Sriram, D.; Yogeewari, P. *ChemMedChem* **2014**, *9*(11), 2538-2547.
- [11]. Hidalgo-Figueroa, S.; Ramirez-Espinosa, J. J.; Estrada-Soto, S.; Almanza-Perez, J. C.; Roman-Ramos, R.; Alarcon-Aguilar, F. J.; Hernandez-Rosado, J. V.; Moreno-Diaz, H.; Diaz-Coutino, D.; Navarrete-Vazquez, G. *Chem. Bio. Drug Des.* **2013**, *81*(4), 474-483.
- [12]. Barros, F. W.; Silva, T. G.; da Rocha Pitta, M. G.; Bezerra, D. P.; Costa-Lotuf, L. V.; de Moraes, M. O.; Pessoa, C.; de Moura, M. A. F.; de Abreu, F. C.; de Lima, M. d. C. A. *Bioorg. Med. Chem.* **2012**, *20*(11), 3533-3539.
- [13]. Decker, M. Design of Hybrid Molecules for Drug Development, Elsevier, ISBN: 978-0-08-101011-2, 2017.
- [14]. Nirwan, S.; Chahal, V.; Kakkar, R. J. *Heterocyc. Chem.* **2019**, *56*(4), 1239-1253.
- [15]. Desai, N.; Joshi, V.; Rajpara, K.; Vaghani, H.; Satodiya, H. *Med. Chem. Res.* **2013**, *22*(4), 1893-1908.
- [16]. War, J. A.; Srivastava, S. K.; Srivastava, S. D. *Spectrochim. Acta A* **2017**, *173*, 270-278.
- [17]. War, J. A.; Srivastava, S. K.; Srivastava, S. D. *Eur. J. Chem.* **2016**, *7*(3), 271-279.
- [18]. War, J. A.; Srivastava, S. K.; Srivastava, S. D. *Luminescence* **2017**, *32*(1), 104-113.
- [19]. Kohanski, M. A.; Dwyer, D. J.; Collins, J. J. *Nature Rev. Microbiol.* **2010**, *8*(6), 423-435.
- [20]. Pindur, U.; Jansen, M.; Lemster, T. *Curr. Med. Chem.* **2005**, *12*(24), 2805-2847.
- [21]. Dar, A. M.; Gato, M. A.; Ahmad, A.; Ahmad, M. S.; Najjar, M. H. J. *Fluoresc.* **2015**, *25*(5), 1377-1387.
- [22]. Paulikova, H.; Vantova, Z.; Hunakova, L.; Cizekova, L.; Carna, M.; Kozurkova, M.; Sabolova, D.; Kristian, P.; Hamulakova, S.; Imrich, J. *Bioorg. Med. Chem.* **2012**, *20*(24), 7139-7148.
- [23]. Shi, J. H.; Liu, T. T.; Jiang, M.; Chen, J.; Wang, Q. J. *Photochem. Photobiol. B: Biol.* **2015**, *147*, 47-55.
- [24]. Dervan, P. B.; Edelson, B. S. *Curr. Opin. Struct. Biol.* **2003**, *13*(3), 284-299.
- [25]. Drew, W. L.; Barry, A.; O'Toole, R.; Sherris, J. C. *Appl. Environ. Microbiol.* **1972**, *24*(2), 240-247.
- [26]. Wiegand, I.; Hilpert, K.; Hancock, R. E. *Nature Prot.* **2008**, *3*(2), 163-175.
- [27]. Molinspiration Cheminformatics, Web server, Retrieved April 01, 2020, from www.molinspiration.com.
- [28]. Molsoft LLC, Web server, Retrieved April 01, 2020, from www.molsoft.com.
- [29]. Frisch, M. J.; Trucks, G. W.; Schlegel, H. B.; Scuseria, G. E.; Robb, M. A.; Cheeseman, J. R.; Scalmani, G.; Barone, V.; Mennucci, B.; Petersson, G. A.; Nakatsuji, H.; Caricato, M.; Li, X.; Hratchian, H. P.; Izmaylov, A. F.; Bloino, J.; Zheng, G.; Sonnenberg, J. L.; Hada, M.; Ehara, M.; Toyota, K.; Fukuda, R.; Hasegawa, J.; Ishida, M.; Nakajima, T.; Honda, Y.; Kitao, O.; Nakai, H.; Vreven, T.; Montgomery, J. A.; Peralta, J. E.; Ogliaro, F.; Bearpark, M.; Heyd, J. J.; Brothers, E.; Kudin, K. N.; Staroverov, V. N.; Kobayashi, R.; Normand, J.; Raghavachari, K.; Rendell, A.; Burant, J. C.; Iyengar, S. S.; Tomasi, J.; Cossi, M.; Rega, N.; Millam, J. M.; Klene, M.; Knox, J. E.; Cross, J. B.; Bakken, V.; Adamo, C.; Jaramillo, J.; Gomperts, R.; Stratmann, R. E.; Yazyev, O.; A. J. Austin, A. J.; Cammi, R.; Pomelli, C.; Ochterski, J. W.; Martin, R. L.; Morokuma, K.; Zakrzewski, V. G.; Voth, G. A.; Salvador, P.; Dannenberg, J. J.; Dapprich, S.; Daniels, A. D.; Farkas, O.; Foresman, J. B.; Ortiz, J. V.; Cioslowski, J.; Fox, D. J. Gaussian, Inc., Gaussian 09, Revision A.02, Wallingford CT, 2009.
- [30]. Trott, O.; Olson, A. J. *J. Comput. Chem.* **2010**, *31*(2), 455-461.
- [31]. Lipinski, C. A.; Lombardo, F.; Dominy, B. W.; Feeney, P. J. *Adv. Drug Deliv. Rev.* **2012**, *64*, 4-17.
- [32]. Ertl, P.; Rohde, B.; Selzer, P. *J. Med. Chem.* **2000**, *43*(20), 3714-3717.
- [33]. Veber, D. F.; Johnson, S. R.; Cheng, H. Y.; Smith, B. R.; Ward, K. W.; Kopple, K. D. *J. Med. Chem.* **2002**, *45*(12), 2615-2623.
- [34]. Auffinger, P.; Hays, F. A.; Westhof, E.; Ho, P. S. *Proc. Natl. Acad. Sci.* **2004**, *101*(48), 16789-16794.
- [35]. Fei, Y.; Lu, G.; Fan, G.; Wu, Y. *Anal. Sci.* **2009**, *25*(11), 1333-1338.
- [36]. Sirajuddin, M.; Ali, S.; Badshah, A. J. *Photochem. Photobiol. B: Biol.* **2013**, *124*, 1-19.
- [37]. Rafique, B.; Khalid, A. M.; Akhtar, K.; Jabbar, A. *Biosens. Bioelectron.* **2013**, *44*, 21-26.
- [38]. Kumar, C. V.; Punzalan, E. H.; Tan, W. B. *Tetrahedron* **2000**, *56*(36), 7027-7040.
- [39]. Wang, T.; Zhao, Z.; Zhang, L.; Ji, L. *J. Mol. Struct.* **2009**, *937*(1-3), 65-69.
- [40]. Baguley, B. *Mol. Cell. Biochem.* **1982**, *43*(3), 167-181.
- [41]. Taylor, R. D.; Jewsbury, P. J.; Essex, J. W. *J. Comput. Aided Mol. Des.* **2002**, *16*(3), 151-166.
- [42]. Ricci, C. G.; Netz, P. A. *J. Chem. Inform. Model.* **2009**, *49*(8), 1925-1935.
- [43]. Shen, G. F.; Liu, T. T.; Wang, Q.; Jiang, M.; Shi, J. H. *J. Photochem. Photobiol. B: Biol.* **2015**, *153*, 380-390.



Copyright © 2020 by Authors. This work is published and licensed by Atlanta Publishing House LLC, Atlanta, GA, USA. The full terms of this license are available at <http://www.eurjchem.com/index.php/eurjchem/pages/view/terms> and incorporate the Creative Commons Attribution-Non Commercial (CC BY NC) (International, v4.0) License (<http://creativecommons.org/licenses/by-nc/4.0>). By accessing the work, you hereby accept the Terms. This is an open access article distributed under the terms and conditions of the CC BY NC License, which permits unrestricted non-commercial use, distribution, and reproduction in any medium, provided the original work is properly cited without any further permission from Atlanta Publishing House LLC (European Journal of Chemistry). No use, distribution or reproduction is permitted which does not comply with these terms. Permissions for commercial use of this work beyond the scope of the License (<http://www.eurjchem.com/index.php/eurjchem/pages/view/terms>) are administered by Atlanta Publishing House LLC (European Journal of Chemistry).